Supporting Information

For

Achieving high-efficient triboelectric nanogenerator *via* a charge reversion process

Ziting Guo,‡[ab] Peiyuan Yang,‡[a] Zhihao Zhao,*[ab] Yikui Gao,[ab] Jiayue Zhang,[a] Linglin Zhou,[ab] Jie Wang,*[ab] and Zhong Lin Wang*[acd]

[a] Beijing Institute of Nanoenergy and Nanosystems, Chinese Academy of Sciences, Beijing 100083, P. R. China

[b] School of Nanoscience and Engineering, University of Chinese Academy of Sciences, Beijing 100049, P. R. China

[c] Georgia Institute of Technology, Atlanta, GA 30332, USA

[d] Yonsei Frontier Lab, Yonsei University, Seoul 03722, Republic of Korea

‡These authors contributed equally to this work.

*** Corresponding Author:**

Z. Zhao: zhaozhihao@binn.cas.cn; J. Wang: wangjie@binn.cas.cn; Z. L.Wang: zhong.wang@mse.gatech.edu.

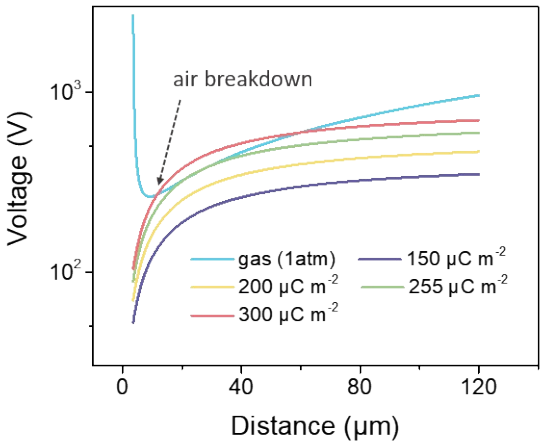

Figure S1. Air breakdown voltage at different distances and gap voltage of TENG with different charge densities (simulation parameters: dielectric film thickness, 50 μm; relative permittivity, 2).

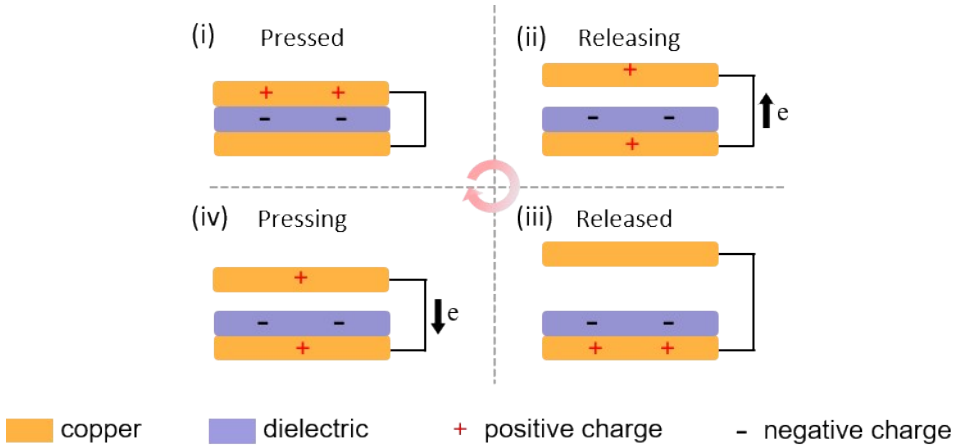

Figure S2. Detailed charge transfer behavior of TENG at original state.

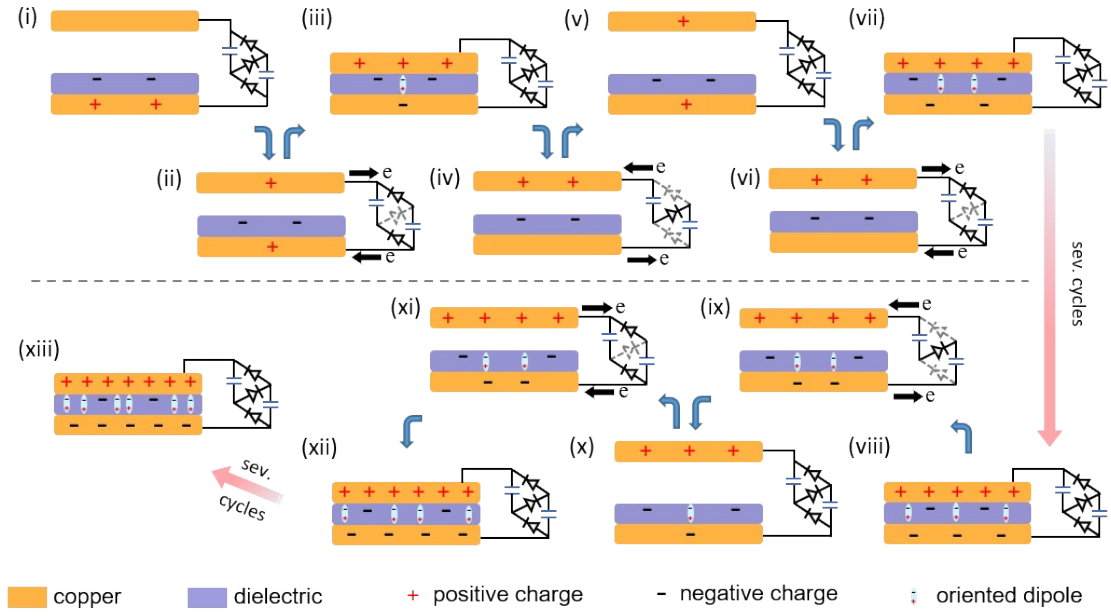

Figure S3. Charge accumulation process of TENG with VMC before air breakdown.

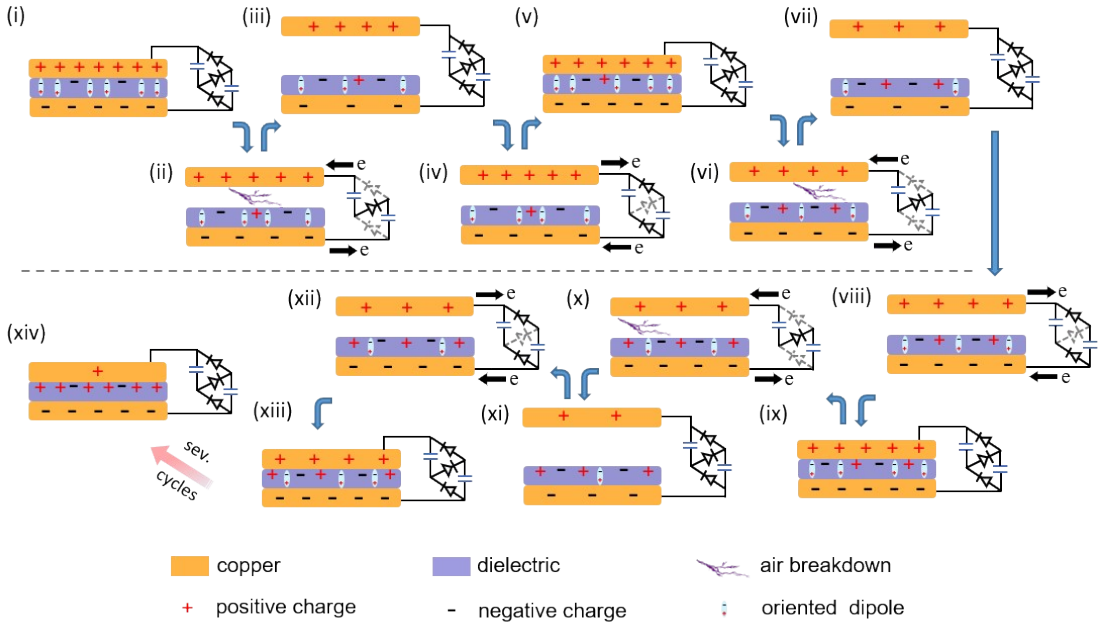

Figure S4. Charge reversion process of TENG with VMC during air breakdown.

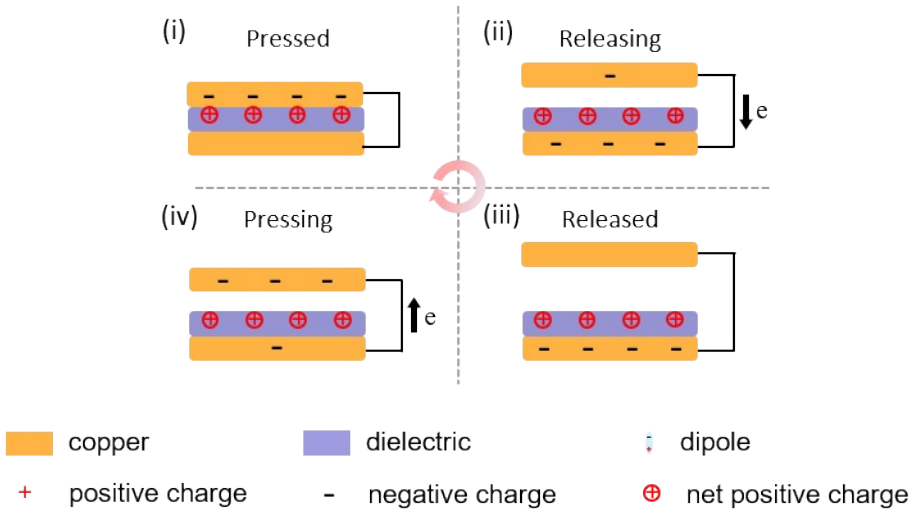

Figure S5. Detailed charge transfer behavior of TENG at net reversed charge state.

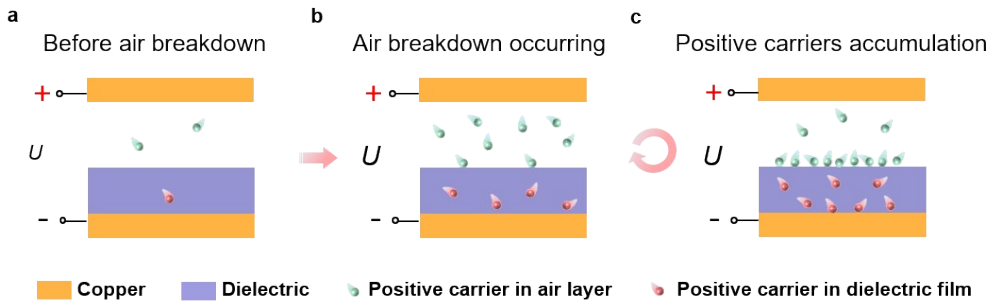

Figure S6. Illustration of positive carrier accumulation process on the dielectric surface. (a) Before air breakdown. (b) The generated carriers on the occurrence of air breakdown. (c) The accumulation of carriers on dielectric surface.

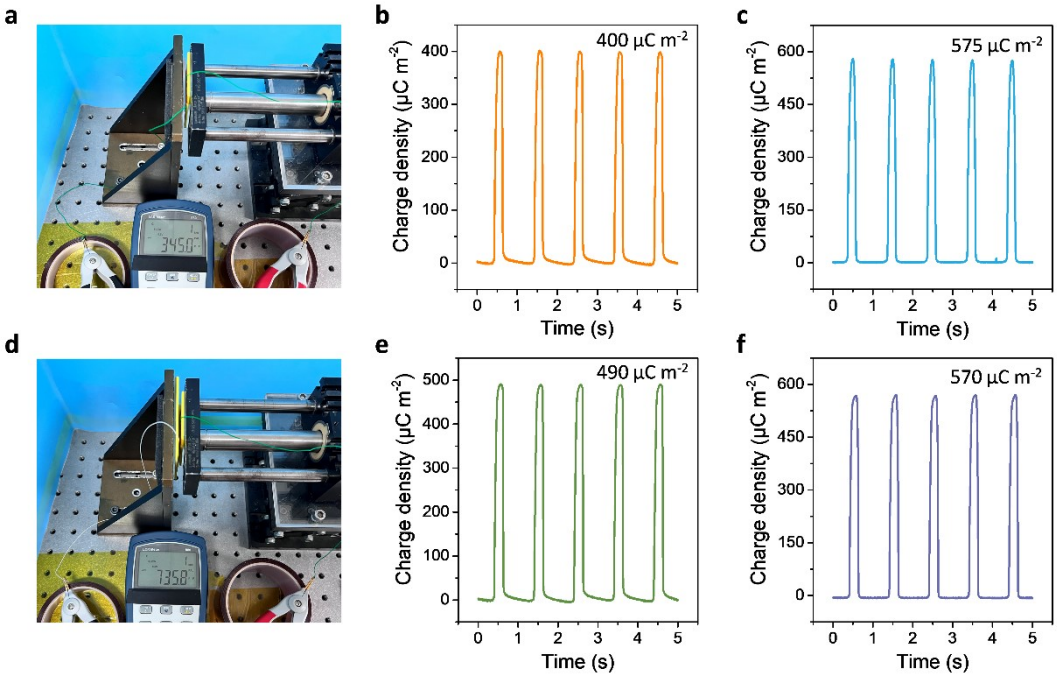

Figure S7. Reversed output of TENG in different contact conditions. (a, b, c) Contact capacitance, maximum output in SCE, and reversed output of TENG with acrylic substrate. (d, e, f) Contact capacitance, maximum output in SCE, and reversed output of TENG with foam and silica-gel substrate.

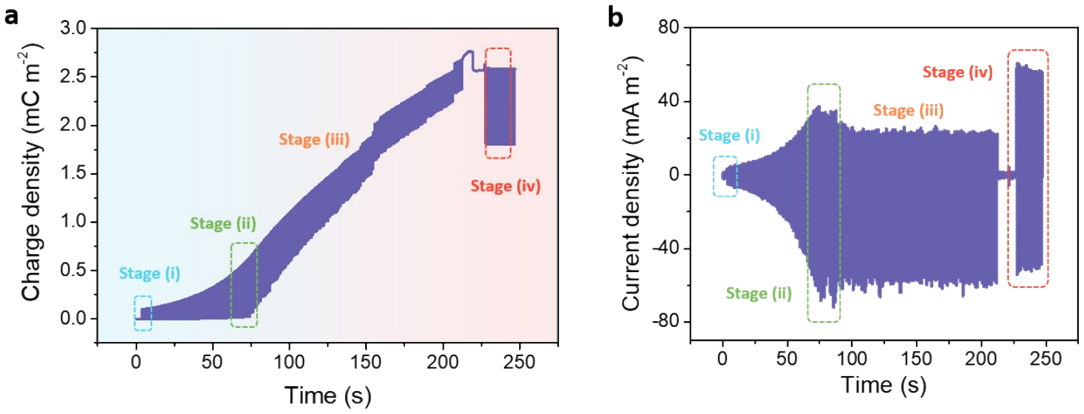

Figure S8. Transfer charge density and current density during the whole process of a TENG with 10 μm PTFE. (a) Transferred charge density of the TENG during the whole process. (b) The corresponding short circuit current density of TENG.

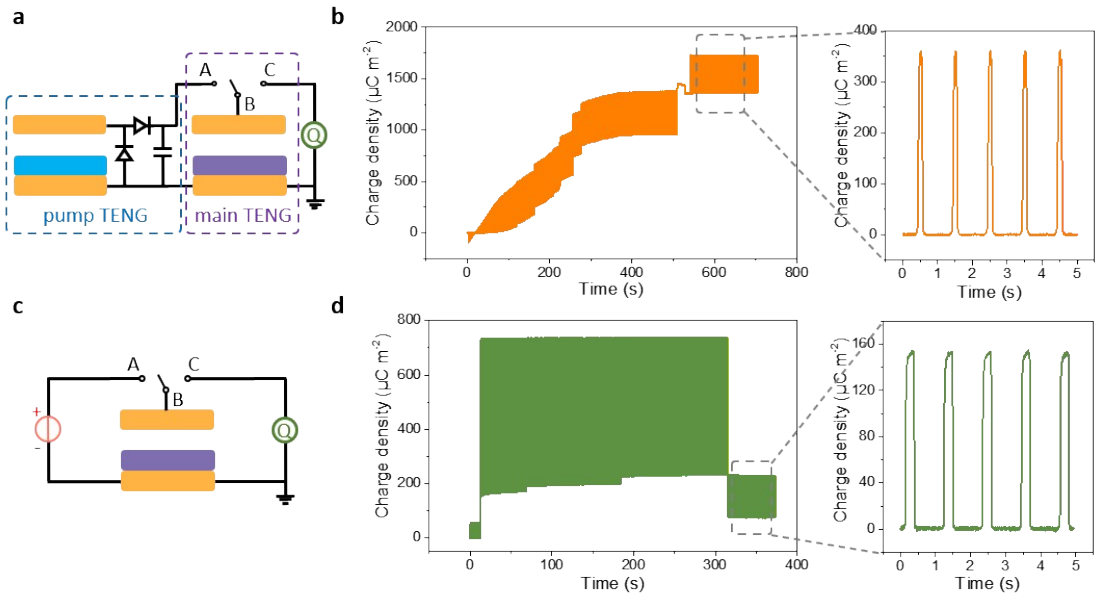

Figure S9. Reversed output of TENG in different electrostatic breakdown phenomena. (a, b) Circuit diagram and output charge density of TENG in external-charge excitation strategy (pump TENG: 30 μm FEP in 4 cm^2). (c, d) Circuit diagram and output charge density of TENG with external high-voltage source (external voltage: 700 V).

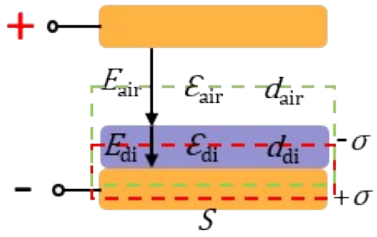

Figure S10. Diagram of selected Gaussian surfaces to calculate the electric flux in TENG.

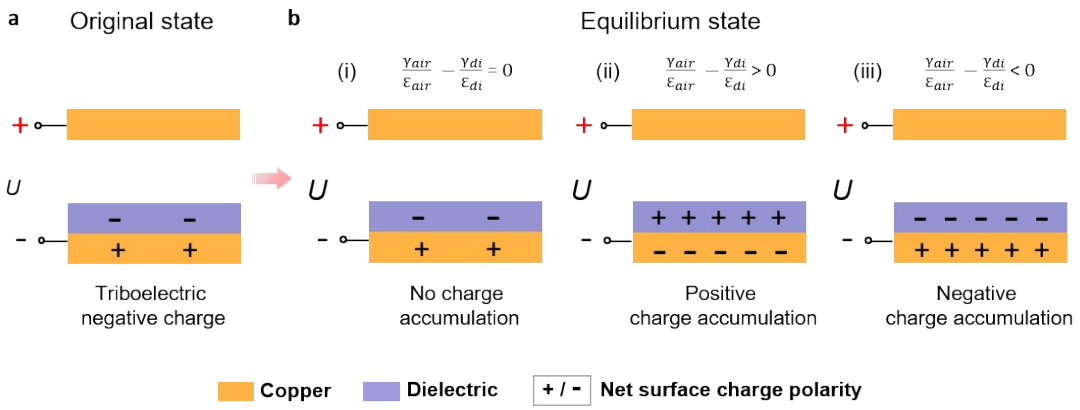

Figure S11. Theoretical analysis of the accumulated charges on dielectric surface at equilibrium state. (a) The original charge distribution for negatively tribo-charged dielectric. (b) The charge distribution for negatively tribo-charged dielectric at the equilibrium state.

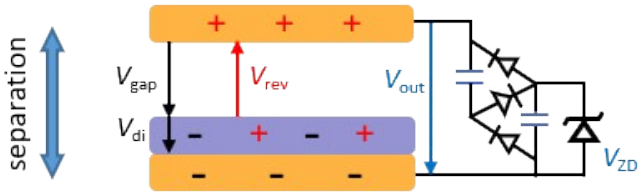

Figure S12. Diagram of different voltages when TENG in separation state.

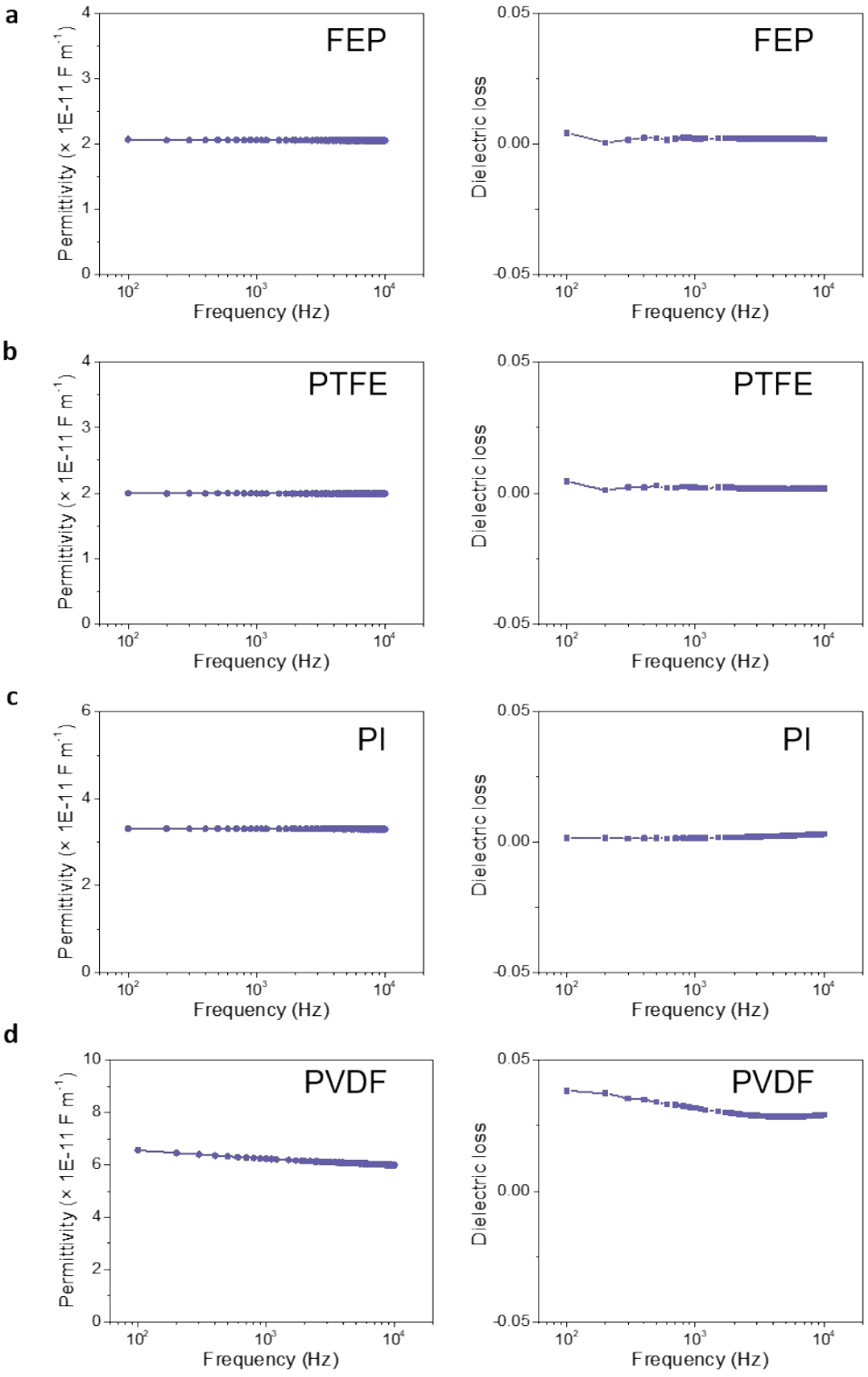

Figure S13. Permittivity and dielectric loss curves of selected dielectrics under different frequencies. (a) Permittivity and dielectric loss curves of 30 μm FEP. (b) Permittivity and dielectric loss curves of 30 μm PTFE. (c) Permittivity and dielectric loss curves of 30 μm PI. (d) Permittivity and dielectric loss curves of 30 μm PVDF.

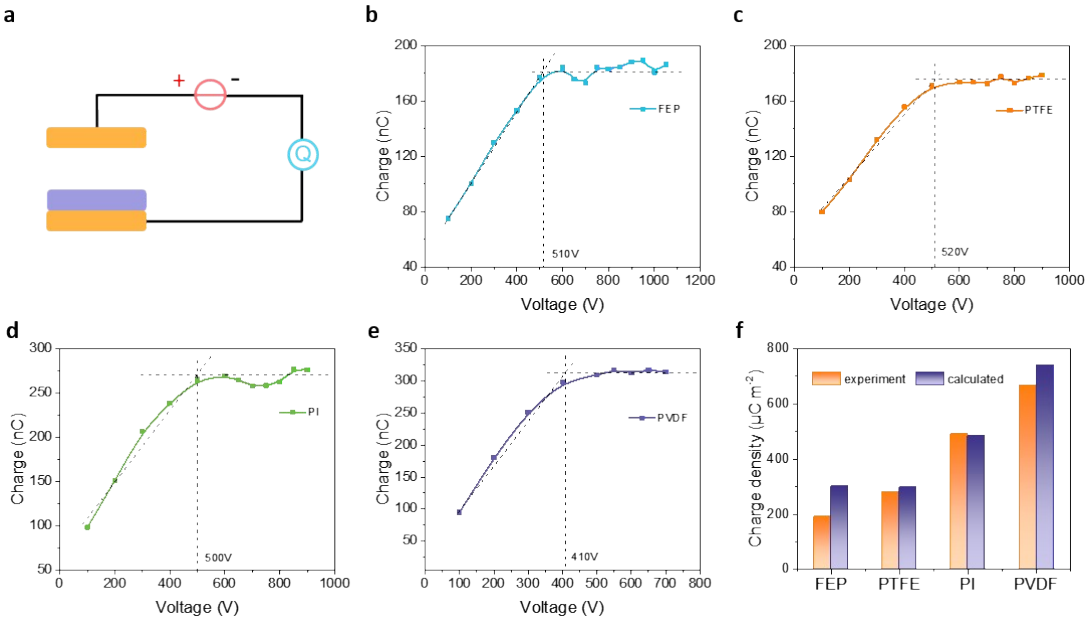

Figure S14. Test method of the theoretical value of reversed charge density and output comparison with experiment results. (a) Circuit diagram to test U_{max}. (b to e) U_{max} of 30 μm FEP, 30 μm PTFE, 30 μm PI, and 30 μm PVDF. (f) Comparison of the output charge densities between experiment results and theoretical results.

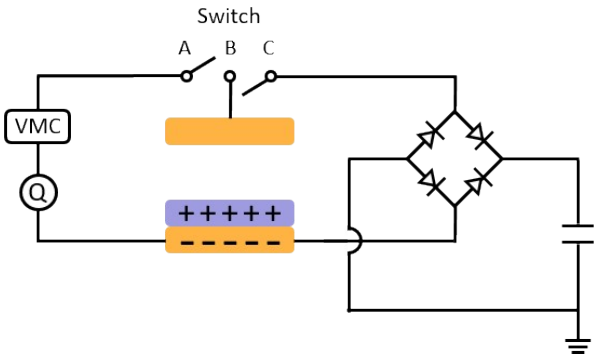

Figure S15. Circuit diagram of capacitor connecting to the TENG after a full-wave rectification without using power management system (PMS).

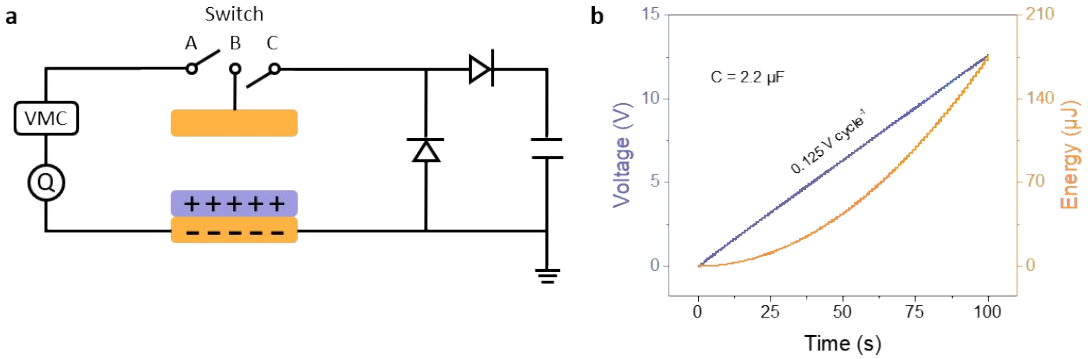

Figure S16. Capacitor connection to the TENG after a half-wave rectification without using PMS. (a) Circuit diagram of the test system. (b) Voltage and energy curves of the capacitor.

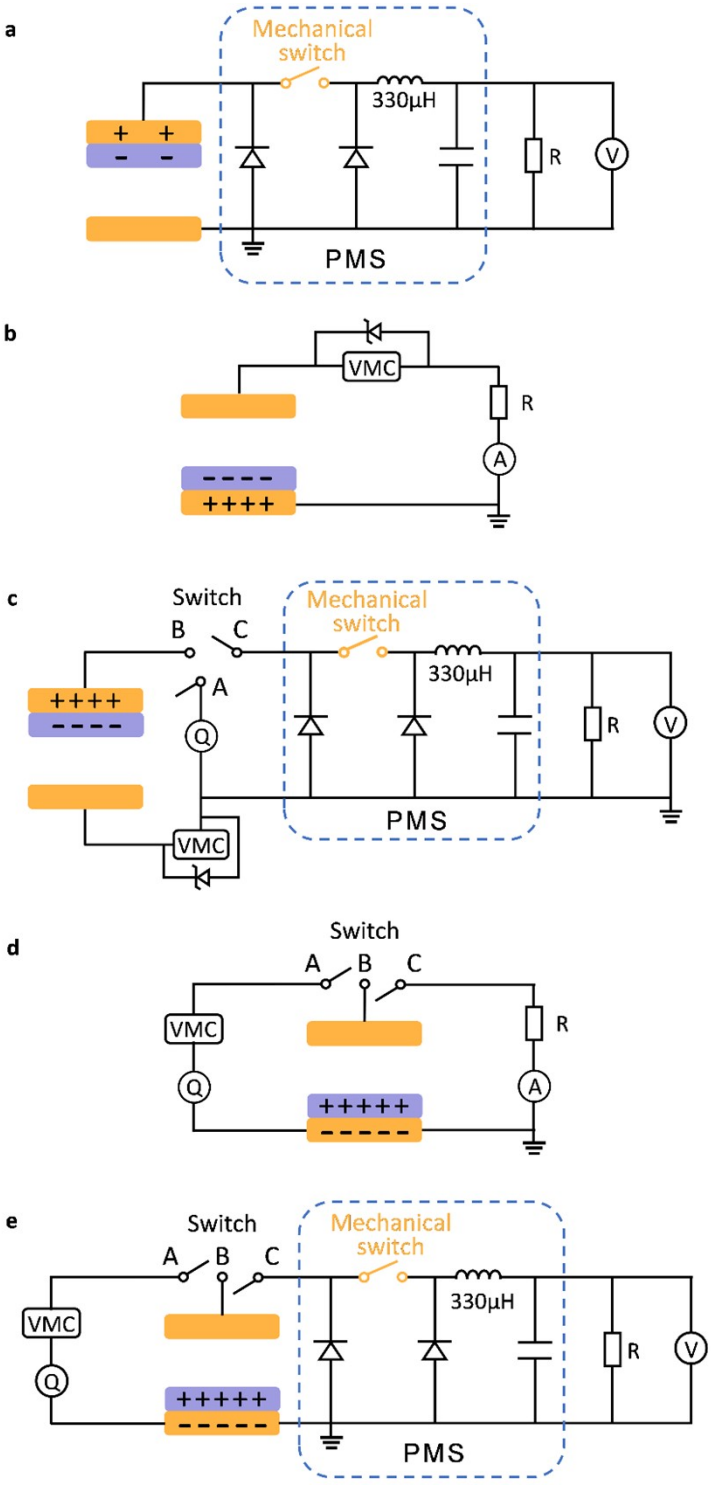

Figure S17. Circuit diagram of TENG charging resistance in different modes. (a) At the original state of TENG without charge excitation process but with PMS (w/o VMC + w/ PMS). (b) With charge excitation process in TENG but without PMS (w/ VMC + w/o PMS, and there is a Zener diode with a stabilized voltage of 500 V). (c) With charge excitation process in TENG and with PMS (w/ VMC + w/ PMS, and there is a Zener diode with a stabilized voltage of 500 V). (d) After charge reversion process in TENG but without PMS (CR + w/o PMS). (e) After charge reversion process in TENG and with PMS (CR + w/ PMS).

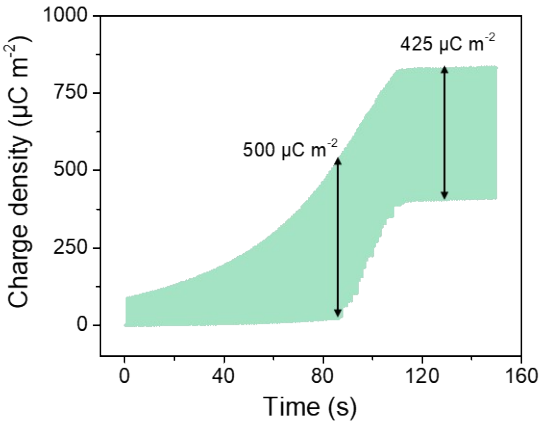

Figure S18. Charge density of a TENG with 10 μm PTFE at the state of "w/ VMC + w/ PMS" with a Zener diode of 500 V.

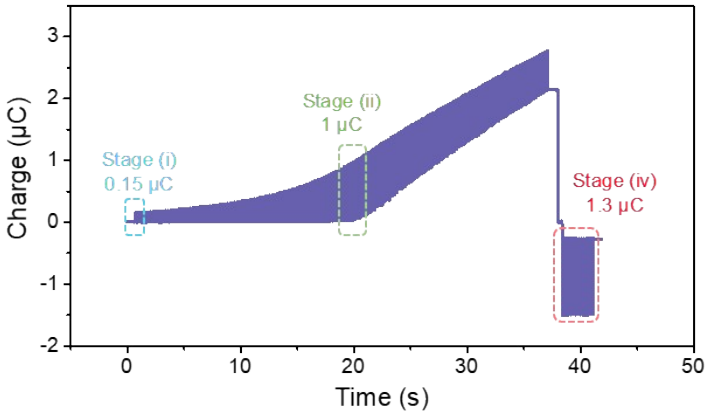

Figure S19. Output charge density of the TENG with 20 μm PTFE and an area of 30 cm^2.

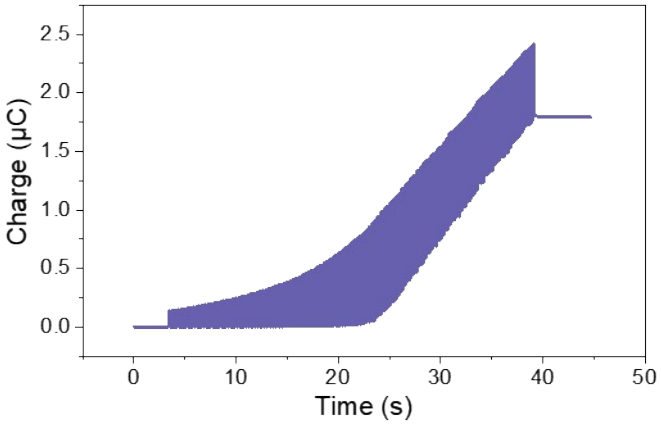

Figure S20. Charge density of the TENG powering a 3*3 hygrothermograph array with the VMC turning on.

Table S1. Conductivity and relative permittivity of different materials.

Material	ρ / Ω m	γ / S m^{-1}	ε / F m^{-1}	γ/ε
FEP	2.28E13	4.38E-14	2.06E-11	2.13E-03
PTFE	2.35E13	4.26E-14	2.00E-11	2.13E-04
PI	6.29E13	1.59E-14	3.30E-11	4.82E-04
PVDF	1.80E13	5.56E-14	6.20E-11	8.97E-04
Air	1.60E12	6.25E-13	8.85E-12	7.06E-02

Where, ρ is the resistivity, γ is the conductivity, and ε is the permittivity of different materials, respectively.

Because $\frac{\gamma_{air}}{\varepsilon_{air}} - \frac{\gamma_{di}}{\varepsilon_{di}} > 0$ for all selected dielectric materials, according to Equation 6, the accumulated charges on dielectric surface will be in reversed polarity (positive), which is consistent with the experimental phenomena.

Note S1. Detailed charge transfer behavior of TENG at original state.

As shown in Figure S2, at the original state, the negative and positive charges are generated on the surface of dielectric film and the upper electrode respectively, based on the triboelectrification effect (state (i)), which are usually scant due to the inadequate triboelectrification limited by an imperfect contact status. Then with the upper electrode releasing from the contact state, the electrons on the bottom electrode are transferred to the upper electrode through the external circuit, generating one output signal, which is actuated by the electrostatic induction effect (state (ii)). And when the release motion is adequate, the electrons transfer is complete (state (iii)). Then the upper electrode is pressed to contacting with the dielectric film, and the electrons on the upper electrode are transferred back to the bottom electrode through the external circuit, generating one opposite-direction output signal, which is also actuated by the electrostatic induction effect (state (iv)). When the press motion is accomplished, the electrons are likewise transferred completely back to the bottom electrode, as depicted in state (i). And one whole alternating-current output is generated in one complete contact-separation motion cycle.

Note S2. Detailed charge transfer behavior of TENG with self-charge excitation circuit before air breakdown.

Self-charge excitation strategy is an effective and extensively used method to boost the output charge density of TENG and overcome the limitation of dielectrics triboelectrification ability, based on the electron transfer and accumulation behavior between the TENG device and the voltage-multiply circuit (VMC) during the contact-separation motion of TENG, in which the VMC is connected to the two electrodes of TENG (the positive terminal of VMC connects to the upper electrode, while the negative terminal connects to the bottom electrode, as shown in the circuit diagram in Figure S3. The tribo-charges on the dielectric film are set to be two negative ones on the dielectric surface, which has been saturated and keep constant during the whole process).

As shown in Figure S3, when the TENG device is pressed to contact (state (i) to (iii)), its capacitance is increasing while its voltage is decreasing, and at the same time, the capacitors in the VMC are connected in parallel (state (ii)), which have a higher voltage and a lower capacitance. Under this condition, the electrons are transferred from the VMC to the TENG bottom electrode, actuated by the difference of voltage (correspondingly, the electrons in the TENG upper electrode are transferred to VMC at the same time). And it is worth noting that, when the TENG is contacted, the electric filed in the dielectric film is enhanced, which results in the dipoles in the film arranging directionally. Then with the releasing motion of the TENG device (state (iii) to (v)), the capacitance of the TENG is decreasing while its voltage is increasing, and at the same time, the capacitors in the VMC become to series-connected (state (iv)), which have a lower voltage and a higher capacitance, and under this condition, the electrons will be transferred from the TENG bottom electrode to VMC, which is actuated by the difference of voltage (correspondingly, the electrons in VMC are transferred to TENG upper electrode). And then, when TENG operates in the next cycle (state (vi) and (vii)), the similar process proceeds once again, at this time, at the moment the TENG contacting (state (vii)), there will be more charges in the electrodes and more oriented dipoles in the dielectric film compared to state (iii), due to the charge transfer and

accumulation behaviors, which is namely the charge excitation effect *via* VMC circuit. After several cycles, there will be more electrons and oriented dipoles in the TENG (state (viii)). And as the similar process performed before, when the TENG is separating, the electrons in TENG bottom electrode will be transferred to VMC, with the electric filed in the dielectric film attenuating, which leads to the oriented dipoles in the film reducing (state (viii) to (x)), while during the contacting process, the electrons will be transferred back to the bottom electrode and increased more, with an enhanced electric field and incremental oriented dipoles in the dielectric, as shown in state (x) to (xii). And this charge accumulation process will keep repeating, until the charges in the electrodes eventually reach the saturated value, as shown in state (xiii), in which more charges in the electrodes will then induce the air breakdown occurring, and result in an attenuated output, as illustrated in Note S3.

Note S3. Detailed charge transfer behavior of TENG with self-charge excitation circuit after air breakdown.

As shown in Figure S4, with the increased charge density in electrodes resulting from the charge excitation effect, the electric field between the upper electrode and the dielectric film in TENG also enhances. Consequently, during the separating motion, once the gap voltage overs the threshold voltage of igniting air breakdown under a certain air gap distance, the electrostatic breakdown of air layer will occur with an instantaneous spark, as shown in state (ii), which leads to the partial air ionization and generates some carriers in the air gap, with a greatly increased air conductivity. Moreover, these carriers will move directionally under the drive of the high excitation voltage constructed from the VMC, resulting in the deposit of positive carriers on the dielectric surface (as depicted in Figure S6), which will reduce the net negative surface charge density of the dielectric, while the negative carriers moving to the upper electrode and neutralizing with the positive charges in it. Meanwhile, the electrons transfer executes at the same time, from the TENG bottom electrode to VMC. So, the oriented dipoles in the dielectric will reduce more under this circumstance (state (ii)) compared to that in Note S2. As the separating motion going continuously, the electrons in the bottom electrode keep transferring to the VMC, and the oriented dipoles in the dielectric film sustain reducing (state (iii)). Then, when the TENG turns to contact, the electrons transfer back from the VMC to the bottom electrode, with the oriented dipoles in the dielectric increasing (state (iii) to (v)), which is similar to the process described in Note S2. It is worth noting that, as the positive charges depositing on the dielectric surface, the electric field of TENG will be reduced, which then will impact the electrons transfer between the TENG and VMC, leading to an impaired excitation effect and a deficient output in the circuit, and this is reflected by the fewer charges in the upper electrode of TENG at state (v) than that of state (i).

Then after several cycles, the charges will anew accumulate in the electrodes of TENG, and the gap voltage between the upper electrode and the dielectric film will over the threshold voltage of igniting air breakdown under a certain gap distance once again, which results in the electrostatic breakdown of air layer one more time, as well as the

partial air ionization, and more positive carriers will deposit on the dielectric surface at this time, reducing the net negative charge density of the dielectric further (state (vi)), with even fewer charges in the upper electrode, and fewer oriented dipoles in the dielectric, which is similar to the state (ii). Then as the TENG move to separate and contact, the electrons transfer behavior performs the same as before, as depicted in state (vii) to (ix).

Then as the electrostatic breakdown occurring repeatedly, more positive carriers will deposit on the dielectric surface, and the net charge density of the dielectric will turn to positive progressively, as shown in state (x) to (xiii), while the oriented dipoles in the dielectric become even fewer, because of the reversed direction of the excitation voltage and the voltage constructed by the deposited positive charges on the dielectric surface, which leads to a weakened net electric filed in the TENG. And finally, when the net electric filed in the TENG is as weak as cannot ignite the air breakdown in the gap furthermore, the positive carriers on the dielectric film will stop to increase, and the output of TENG will then become stable and stop further reducing, as shown in state (xiv), in which there are usually few charges in the upper electrode of TENG, with a severely damaged charge excitation effect and an extremely low output in the circuit.

Note S4. Detailed charge transfer behavior of TENG with reversed charges.

As shown in Figure S5, with the abundant deposited positive charges on the dielectric surface, the net surface charge density of the dielectric finally becomes to positive, as documented in Note S3. And in this circumstance, if the excitation voltage is revoked, the net positive charges on the dielectric surface will then dominate the TENG output, as depicted in state (i) above, with a similar electrostatic induction process of the original condition, but the net positive charges in the dielectric, and negative charges in the electrodes: when the TENG is separating, the electrons in the upper electrode transfer to the bottom one through the external circuit (state (i) to (iii)), and which then transfer back to the upper electrode during the contacting process (state (iii) to (i)).

Whereas, a significantly improved output can be achieved compared to the original condition. Because at the original state, the charges generated by triboelectrification effect is related to the contact efficiency of TENG, and due to the surfaces of dielectric film and electrodes are both rough in practical devices, their contact status and triboelectrification effect are both inadequate, which results in an impaired output in the external circuit, as documented in Note S1 and illustrated in Figure 1C. However, when air breakdown occurs, the charges are generated by the electrostatic breakdown effect, distributed uniformly in the whole space, and then move directionally to accumulate on the dielectric surface, which is independent to the contact efficiency, as shown in Figure S6, therefore more charges can be accumulated, and a signally higher output is achieved.

Note S5. Difference of the effect of materials' contact efficiency on charge reversion process and charge excitation process.

In SCE strategy, the electrons are transferred between TENG electrodes and the VMC. Then the charges in electrodes increase gradually. During the periodic contact-separation motion, the charges on dielectric surface also increase due to the electrostatic induction effect, which then together with the charges in upper electrode collectively build a voltage in the air layer of TENG. Once the voltage over the breakdown threshold given by Paschen's Law, the electrostatic breakdown effect will occur in air, and the output of TENG stops to increase further. Considering that the surfaces of both upper electrode and dielectric film are rough in practical devices, the real contact state between them is in a point-to-point manner, rather than a face-to-face way, so the contact efficiency of TENG is impaired (defined as the ratio of actual effective contact area of electrode to the whole area of electrode), which leads the electrostatic breakdown process easier to occur. As a result, the charge density of TENG in SCE strategy will not meet the theoretical value given by Paschen's Law, as shown in Fig. 1e and Fig. 2g in the text. That is, the TENG performance in SCE strategy is limited by the contact efficiency of materials.

On the other hand, it is worth noting that the electrostatic breakdown process carries out in a space field, which is different from the electrostatic induction effect in a point-to-point way. The breakdown has no strict and clear spatial boundary, and so are the generated air carriers. As a result, under the drive of the electric field, the reversed charges deposited on dielectric surface can over the induced charges in SCE strategy, as shown in Fig. 1d and Fig. 2g in text. In other words, the limitation of the contact efficiency is broken in the charge reversion process, and the reversed charges are independent of materials' contact efficiency.

Moreover, to confirm this statement, some experiments are also carried out. Different substrates are utilized under the dielectric film to control the TENG contact efficiency (acrylic, and foam and silica-gel are respectively used as substrates under a 10 μm PTFE film), then the charge reversion process is conducted. The results are displayed in Figure S7. According to the tested capacitances of TENG, the contact efficiencies are

calculated as 43% for acrylic substrate, and 92% for foam and silica-gel substrate, respectively. The calculation follows by:

$$C_{theory} = \frac{\varepsilon S}{d} = \frac{2 \lozenge 10^{-11} \lozenge 4 \lozenge 10^{-4}}{10 \lozenge 10^{-6}} = 8 \lozenge 10^{-10}\ F = 800\ pF \quad \text{(S1)}$$

$$\eta_{ct} = \frac{C_{test}}{C_{theory}} \lozenge 100\% \quad \text{(S2)}$$

Where, ε, S, and d are the permittivity, area and thickness of the dielectric film, respectively, while C_{test} and C_{theory} are the tested and theoretical capacitance of TENG device, respectively. The results demonstrate that when the TENG has different contact efficiencies, it shows distinct outputs in SCE strategy (400 μC m^{-2} for 43% contact efficiency, and 490 μC m^{-2} for 92% contact efficiency), while the reversed output has no significant difference about 570 μC m^{-2}, which effectively confirms that the charge reversion process is independent of materials' contact efficiency, differing from the charge excitation process.

Note S6. Reason for reversed charge density over the threshold of Paschen's Law.

The threshold of surface charge density of TENG limited by air breakdown can be calculated according to Paschen's Law as:

$$\sigma < \frac{AP(\varepsilon_{air} d_{di} + \varepsilon_{di} d_{air})}{d_{di}[\ln(P d_{air}) + B]} \quad \text{(S3)}$$

where P is the air pressure, d_{air} is the air gap distance, d_{di} is the dielectric film thickness, A (2.87×10^7 V·atm^{-1}·m^{-1}) is a constant associated with the ionization and excitation energies of metal electrodes, as well as the humidity, type, and other characteristics of the surrounding atmosphere, and B (12.6) is a constant related to the secondary-electron-emission coefficient (the number of secondary electrons produced per incident positive ion) of the metal electrodes. Considering that the equation is a semi-empirical formula, while the reversed charges are generated by the partial breakdown of air layer and then accumulate directionally on the dielectric surface, which distribute more uniformly than the tribo-charges, as described in Note S4, the reversed charges may have a higher threshold, resulting that its density is over the threshold value given by Paschen's Law.

Note S7. The general relationship of charge reversion process on electrostatic breakdown effect.

The electrostatic breakdown effect is a universal phenomenon occurring in many conditions, as long as the voltage in air layer meet the breakdown threshold given by Paschen's Law. To demonstrate that the charge reversion process has a general dependence on electrostatic breakdown effect, the revered outputs of TENG in external-charge excitation (ECE) strategy and in the condition with external high-voltage source are also tested, as presented in Figure S9. From the experiment results, it can be seen that, in other conditions where electrostatic breakdown occurs, the charge reversion process also carries out, which indicates that the charge reversion process has a general dependence on electrostatic breakdown effect. In this work, considering that SCE strategy is a commonly used method to enhance the surface charge density of TENG, and it enables a rapid voltage increase process based on the role of VMC, which can thereby induce sufficient electrostatic breakdown effect, the charge reversion experiments are conducted in this way. However, the SCE strategy is only one of the methods to achieve the air breakdown effect and the resulting charge reversion process, while ECE and other strategies can also realize the same phenomena, attributing to the general relationship between the charge reversion process and the electrostatic breakdown effect.

Note S8. Theoretical analysis of surface charge density of TENG dielectric film with an excitation voltage in the ideal dielectric capacitance model.

According to Gauss theorem and the selected Gaussian surfaces as depicted in Figure S10, the electric flux follows:

$$\oint \vec{D} d\vec{S} = \oint \vec{D_{air}} d\vec{S} = \varepsilon_{air} \vec{E}_{air} d\vec{S} = \oint \vec{D_{di}} d\vec{S} = \varepsilon_{di} \vec{E}_{di} d\vec{S} = \sum_i Q_i = \sigma S = Q \tag{S4}$$

Where D is the electric displacement, S is the integral area, σ is the surface charge density of the electrode and dielectric film, Q is the amount of surface charges, ε_{air}, E_{air} and D_{air} are the permittivity, electric field intensity and electric displacement of air layer, respectively, while ε_{di}, E_{di} and D_{di} are the same parameters of dielectric film. From Equation S4, the relation between the electric field intensities of air layer and dielectric film can be deducted as:

$$\frac{E_{air}}{E_{di}} = \frac{\varepsilon_{di}}{\varepsilon_{air}} \tag{S5}$$

With an applied excitation voltage, the relation between different voltages is:

$$U = V_{air} + V_{di} = E_{air} d_{air} + E_{di} d_{di} \tag{S6}$$

Where U is the excitation voltage given by voltage-multiply circuit, V_{air} and d_{air} are the voltage and thickness of air layer, respectively, while V_{di} and d_{di} are the same parameters of dielectric film. Then combining with Equation S5, E_{di} can be expressed as:

$$E_{di} = \frac{\varepsilon_{air}}{\varepsilon_{di} d_{air} + \varepsilon_{air} d_{di}} U \tag{S7}$$

Thus, the amount of surface charge density of the dielectric film can be derived as:

$$\sigma = \frac{Q}{S} = \varepsilon_{di} E_{di} = \frac{U}{d_{air}/\varepsilon_{air} + d_{di}/\varepsilon_{di}} \tag{S8}$$

Therefore, it can be seen that only the permittivity and thickness of air layer and dielectric film need to be considered to calculate the SCD of dielectric film with an excitation voltage in the conventional ideal dielectric capacitance model.

Note S9. Theoretical analysis of accumulated charge density of TENG with an excitation voltage in the modified dielectric capacitance model.

Though the conduction current densities of air layer and dielectric film are unequal as described in the text, the total current densities are equal according to the Gauss theorem:

$$j_t = j_c + j_d = \gamma_{air}E_{air} + \varepsilon_{air}\frac{dE_{air}}{dt} = \gamma_{di}E_{di} + \varepsilon_{di}\frac{dE_{di}}{dt} \quad \text{(S9)}$$

Where j_t, j_c and j_d are the total current density, conduction current density and displacement current density, respectively, while γ_{air} and γ_{di} are the conductivities of air layer and dielectric film, respectively. Combining with Equation S6, the electric field intensities of air layer and dielectric film can be given by:

$$E_{air}(t) = \frac{\gamma_{di}}{d_{air}\gamma_{di} + d_{di}\gamma_{air}}U + \left(\frac{\varepsilon_{di}}{d_{air}\varepsilon_{di} + d_{di}\varepsilon_{air}} - \frac{\gamma_{di}}{d_{air}\gamma_{di} + d_{di}\gamma_{air}}\right)Ue^{-\frac{t}{\tau}} \quad \text{(S10)}$$

$$E_{di}(t) = \frac{\gamma_{air}}{d_{air}\gamma_{di} + d_{di}\gamma_{air}}U + \left(\frac{\varepsilon_{air}}{d_{air}\varepsilon_{di} + d_{di}\varepsilon_{air}} - \frac{\gamma_{air}}{d_{air}\gamma_{di} + d_{di}\gamma_{air}}\right)Ue^{-\frac{t}{\tau}} \quad \text{(S11)}$$

Where $\tau = \frac{d_{air}\varepsilon_{di} + d_{di}\varepsilon_{air}}{d_{air}\gamma_{di} + d_{di}\gamma_{air}}$ (S12)

Associating with Equation 4 and 5 in the main text, the difference of conduction current densities at the interface can be expressed as:

$$\Delta j_c(t) = j_{c,air}(t) - j_{c,di}(t) = \frac{\gamma_{air}\varepsilon_{di} - \gamma_{di}\varepsilon_{air}}{d_{air}\varepsilon_{di} + d_{di}\varepsilon_{air}}Ue^{-\frac{t}{\tau}} \quad \text{(S13)}$$

Thus, the charges accumulated at the interface over time per unit area is:

$$\sigma = \int_0^\infty \Delta j_c(t)dt = \int_0^\infty \left(j_{c,air}(t) - j_{c,di}(t)\right)dt = \frac{\gamma_{air}\varepsilon_{di} - \gamma_{di}\varepsilon_{air}}{d_{air}\gamma_{di} + d_{di}\gamma_{air}}U = \frac{\varepsilon_{air}\varepsilon_{di}\left(\frac{\gamma_{air}}{\varepsilon_{air}} - \frac{\gamma_{di}}{\varepsilon_{di}}\right)}{d_{air}\gamma_{di} + d_{di}\gamma_{air}}U \quad \text{(S14)}$$

Which is shown as Equation 6 in the text. It can be found that, in the real condition, not only the permittivity and thickness of air layer and dielectric film are need to be considered to calculate the SCD of dielectric film under an excitation voltage, but also their conductivities are effective.

Note S10. Interpretation for charge reversion phenomenon in low-voltage condition.

According to the result displayed in Fig. 2a, when the voltage of VMC is limited to a low value, the output of TENG is also reduced gradually to become reversed, implying that the electrostatic breakdown effect and charge reversion process also execute in the low-voltage region. For this phenomenon, there are three possible reasons:

On one hand, as we all known, the electrostatic breakdown phenomenon normally occurs in high voltage, which is usually true in the case of breakdown happening in an even and flat space. While in practical conditions, both the surfaces of the upper electrode and dielectric film in TENG are uneven, which will result in a locally reinforced electric field in air gap and increase the feasibility of random breakdown behavior under low voltages. Thus, this will might be one of reasons for the weak charge reversion phenomenon under low external voltage in Fig. 2a.

On the other hand, considering that the conductivity of air (γ_{air}, 6.25E-13 S m^{-1}) is always higher than that of dielectric material (γ_{di}, 4.26E-14 S m^{-1} for 10 μm PTFE), even in the case without air breakdown, then according to Equation 6 in the text (Equation S14 in Note S9), the accumulated charges on dielectric surface are always tend to reversed polarity ($\sigma > 0$). As a result, the charge reversion phenomenon is possible to conduct in low-voltage condition which even is hard to occur air breakdown. However, it should be pointed out that, according to the time constant (τ) of charge reversion process in Equation S12 in Note S9, when the voltage (U) is relatively low, the γ_{air} is extremely inferior, which leads the time constant (τ) is greatly long, and the charge reversion process is slow. Meanwhile, the accumulated reversed charges on dielectric surface at this time are few. So, the net surface charges of the dielectric may not change to the reversed polarity, and only a slight decrease of the output charge can be observed, which is consistent with the experiment results when using 60 V and 82 V Zener diodes, as displayed in Fig. 2a. While in the case when air breakdown happening in a higher voltage, the γ_{air} is increased, and the τ is very short. Consequently, the amount of the accumulated reversed charges is improved, with a rapid charge reversion process. And then, the net surface charges of the dielectric in this condition

may gradually invert to the reversed polarity, which coincides with the experiment results when using 100 V, 120 V, and 150 V Zener diodes, as displayed in Fig. 2a. Moreover, due to the deposition of reversed charges on dielectric surface, there will be a reversed voltage in air gap (V_{rev}) that weakens the gap voltage (V_{gap}) as shown in Figure S12. Then the relation of different voltages displayed in the diagram can be expressed as,

$$V_{gap} + V_{di} - V_{rev} = V_{out} \tag{S15}$$

where, V_{di} and V_{out} are respectively the divided voltage of dielectric film and the output voltage of TENG when TENG is in the separation state. And V_{out} is controlled by Zener diodes at this time, that is

$$V_{out} = V_{ZD} \tag{S16}$$

where, V_{ZD} is the working voltage of Zener diodes. Considering that V_{di} is always extremely low that can be ignored, we can get the following relation,

$$V_{gap} \approx V_{rev} + V_{ZD} \tag{S17}$$

From above equation, it can be seen that the gap voltage is actually higher than the Zener diode working voltage during the TENG separation motion, attributing to the deposited reversed charges. Thus, when using a Zener diode with low working voltages, the gap voltage might be high enough to invoke the electrostatic breakdown effect in air, and induce a potential charge reversion phenomenon.

Note S11. Interpretation for the difference of stored energy in C_s per cycle with and without using PMS.

When with PMS, the C_s connects to TENG with an inductor (Fig. 4a). In this condition, due to the quantitative energy output of the inductor per cycle, the stored energy in C_s is nearly constant in one cycle. While in the case without PMS, the C_s connects to TENG after a full-wave rectification (Fig. S15, ESI). At this time, due to the quantitative charge output of TENG in each cycle, the voltage increase of C_s per cycle is nearly constant, and the stored energy of C_s in each cycle can be calculated as follow:

$$V_n = n \cdot \Delta V \tag{S18}$$

$$V_{n+1} = (n+1) \cdot \Delta V \tag{S19}$$

$$E_n = \frac{1}{2} C \cdot V_n^2 = \frac{n^2}{2} C \cdot \Delta V^2 \tag{S20}$$

$$E_{n+1} = \frac{1}{2} C \cdot V_{n+1}^2 = \frac{(n+1)^2}{2} C \cdot \Delta V^2 \tag{S21}$$

$$\Delta E_{n+1} = E_{n+1} - E_n = \frac{2n+1}{2} C \cdot \Delta V^2 = \frac{2(n+1)-1}{2} C \cdot \Delta V^2 \tag{S22}$$

which is equal to

$$\Delta E_n = \frac{2n-1}{2} C \cdot \Delta V^2 \tag{S23}$$

where, n is the cycle number, ΔV is the voltage increase of C_s per cycle, V_n and V_{n+1} respectively are the voltages of C_s after charging n and n+1 cycles, C is the capacitance of C_s, E_n and E_{n+1} respectively are the energies stored in C_s after charging n and n+1 cycles, ΔE_n and ΔE_{n+1} respectively are the energies stored by C_s during the n and n+1 cycles. From above deduction, it can be seen that the stored energy is C_s per cycle is proportional to the cycle number. That is, with the cycle number increases, the stored energy in C_s per cycle will increase linearly, which is different from the case that with PMS.

Note S12. Theoretical analysis of the increase of average power density after power management.

The average power density is measured under a resistive load, and when the load is extremely large, the transfer of charges (electrons) in external circuit could be impeded, leading to a reduced output energy of TENG in per cycle, as well as an impaired output power density. Whereas, when the load is relatively low, the charges (electrons) are easier to transfer through the external circuit, which results in a decreased loss of the output energy and power. Consequently, there is a specious increase of the average output power density after the power management, accompanied by a seemingly more than 100 % efficiency of PMS, due to the incomplete charge transfer at large resistance.